International Journal of Bifurcation and Chaos, Vol. 17, No. 5 (2007) 1589–1598

DIFFUSIVE TRANSPORT THROUGH A NONTWIST BARRIER IN TOKAMAKS

J. S. E. PORTELA and I. L. CALDAS
Instituto de Física, Universidade de São Paulo,
C.P. 66318, 05315-970, São Paulo, São Paulo, Brazil

R. L. VIANA
Departamento de Física, Universidade Federal do Paraná,
C.P. 19081, 81531-990, Curitiba, Paraná, Brazil

P. J. MORRISON
Department of Physics and Institute for Fusion Studies,
University of Texas at Austin, Austin, TX 78712, USA

Received November 10, 2005; Revised April 20, 2006

The magnetic field line structure of tokamaks with reversed magnetic shear is analyzed by means of a nontwist map model that takes into account non-integrable perturbations that describe ergodic magnetic limiters. The map studied possess behavior expected of the standard nontwist map, a well-studied map, despite the different symmetries and the existence of coupled perturbations. A distinguising feature of nontwist maps is the presence of good surfaces in the reveresed shear region, and consequently the appearance of a transport barrier inside the plasma. Such barriers are observed in the present model and are seen to be very robust. Very strong perturbations are required to destroy them, and even after breaking, the transport turns out to be diffusive. Poloidal diffusion is found to be two orders of magnitude higher than radial diffusion.

Keywords: Tokamaks; transport; chaos; nontwist.

1. Introduction

Plasmas confined in toroidal configurations with axisymmetric magnetic fields have field line structure governed by Hamilton's equations, with the toroidal angle playing the role of time. Consequently, the lore of Hamiltonian dynamics has been developed applied to and in conjunction with such configurations. For example, the field lines of axisymmetric equilibria lie on nested toroidal surfaces, constituting integrable Hamiltonian systems, and perturbations of such axisymmetric equilibria are naturally described by Poincaré sections, the intersection of field lines with a poloidal section. Thus the structure of field lines can be understood by studying the repeated mapping of field lines onto this section [Morrison, 2000; Lichtenberg & Lieberman, 1992]. When the safety factor, the helical pitch with which the magnetic field winds around the torus, is a monotonic function of the radius, we have a *twist* map; when this is not true, for example when the safety factor has a maximum, we have a *nontwist* map [Egydio de Carvalho & Osório de Almeida, 1992; del-Castillo-Negrete & Morrison, 1993; Oda & Caldas, 1995; Davidson *et al.*, 1995; Corso *et al.*, 1997; Wurm *et al.*, 2005]. Due to many important results, such as the KAM, Poincaré-Birkhoff, and Aubry–Mather theorems, having proofs only for twist systems, nontwist maps can have new phenomena, such as reconnection of separatrices (e.g. [Howard & Hohs, 1984;

del-Castillo-Negrete & Morrison, 1993]) and new universal behavior of invariant torus destruction [del-Castillo-Negrete *et al.*, 1997].

In tokamaks (the most promising devices for the magnetic confinement of fusion plasmas) nontwist dynamics occurs for hollow toroidal current profiles, which can now be obtained by many experimental techniques, and such profiles are related to enhanced confinement [Levinton *et al.*, 1995; Strait *et al.*, 1995; Mazzucato *et al.*, 1996]. It has been proposed that this better confinement is due to a transport barrier that is characteristic of the nonmonotonic dynamics [Mazzucato *et al.*, 1996]. The main goal of this paper is to study this barrier and the transport through it. We consider an analytically obtained map, replacing lengthy numerical integrations of the magnetic field line of ordinary differential equations by faster iterations, allowing the long-term behavior to be studied. We also use a simplified coordinate system that describes the tokamak edge region.

The paper is organized as follows: in Sec. 2 we introduce the tokamak geometry and the model we use for numerical analyses; in Sec. 3 we present results about the invariant barrier formed by invariant tori that arise; then, in Sec. 4 we describe the transport through the effective barrier that remains after the invariant tori break; in Sec. 5 we find a local approximation for the model and compare it with the standard nontwist map; and finally we conclude in Sec. 6.

2. The Nontwist Map

The basic toroidal geometry of a tokamak is described by its major and minor radii, R_0 and b, respectively. When the tokamak aspect ratio, R_0/b, is large enough one can neglect the effect of the toroidal curvature and treat the system as a periodic cylinder of length $2\pi R_0$, where the symmetry axis is parameterized by the coordinate $z = R_0\phi$ with the toroidal angle ϕ (Fig. 1) [Wesson, 1987]. In this case, the equilibrium toroidal field $B_\phi = B_0$ is nearly uniform (a toroidal correction will be introduced later on). Accordingly, a point in the tokamak is determined by its cylindrical coordinates (r, θ, z) with respect to the symmetry axis. When studying the region near the tokamak wall, it turns out that even the poloidal curvature does not influence results noticeably, consequently a rectangular system can be used with the following coordinates: $x' = b\theta$ and $y' = b - r$ [Martin & Taylor, 1984].

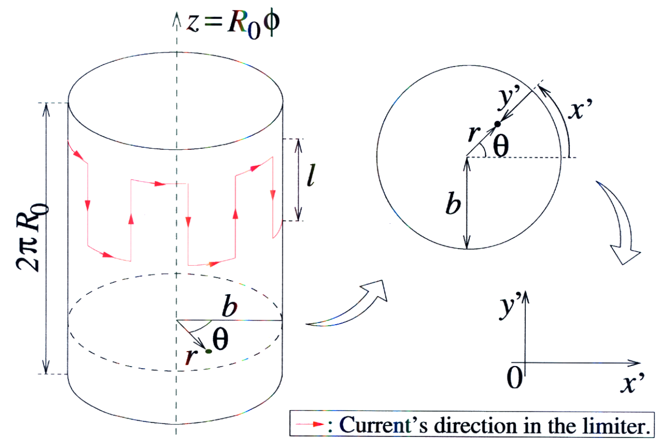

Fig. 1. Schematic view of a tokamak in the periodic cylinder approximation. Shown are its section and the rectangular coordinates (before normalization) used to describe magnetic field lines.

In these coordinates the tokamak wall is thus characterized by the line segment $y' = 0$, extending from $x' = 0$ to $2\pi b$. In the following, we will use mostly the normalized coordinates $x = x'/b$ and $y = y'/b$.

The main magnetic fields of a tokamak are in the toroidal and poloidal directions ($\hat{\phi}$ and $\hat{\theta}$ of Fig. 1) and are generated by external coils and the toroidal plasma current, respectively [Wesson, 1987]. For a given equilibrium magnetic field, the field lines are determined by

$$\mathbf{B} \times \mathrm{d}\mathbf{l} = 0, \tag{1}$$

which in cylindrical coordinates is equivalent to the following:

$$\frac{\mathrm{d}r}{B_r} = \frac{r\mathrm{d}\theta}{B_\theta} = \frac{R_0\mathrm{d}\phi}{B_\phi} = \frac{\mathrm{d}z}{B_\phi}. \tag{2}$$

The equilibrium magnetic field configuration we consider has a toroidal correction given by the a_1 terms in Eqs. (3) and (4). In addition to the equilibrium fields, a perturbative resonant field can be added to control plasma-wall interactions [Karger & Lackner, 1977; Caldas *et al.*, 2002].

As noted above, the structure of the magnetic field lines in a tokamak can be more easily appreciated by examining a Poincaré surface of section, which we take at the plane $z = 0$. We let (r_n, θ_n) be the coordinates of the nth piercing of a given field line with that surface. These coordinates are related to the cartesian coordinates (x, y) introduced above. Because the magnetic field line equations uniquely determine the position of the next piercing, we have a Poincaré map. Due to the solenoidal character of the magnetic field, this map is area-preserving in the surface of section (e.g. [Morrison, 2000]). In a rectangular description, this map can be modeled by an explicit map derived from a generating function [Ullmann & Caldas, 2000]. Thus, the equilibrium magnetic field lines can be described by:

$$r_{n+1} = \frac{r_n}{1 - a_1 \sin\theta_n}, \tag{3}$$

$$\theta_{n+1} = \theta_n + \frac{2\pi}{q_{\mathrm{eq}}(r_{n+1})} + a_1 \cos\theta_n, \tag{4}$$

where the parameter a_1 gives the strength of the toroidal correction and is set as -0.04 as in a previous work [Portela *et al.*, 2007]. We denote this map by $(r_{n+1}, \theta_{n+1}) = \mathbf{T}_e(r_n, \theta_n)$.

In Eq. (4) the function $q_{\mathrm{eq}}(r)$ corresponds to the equilibrium safety factor defined by

$$q_{\mathrm{eq}}(r) = \left\langle \frac{\mathrm{d}\phi}{\mathrm{d}\theta} \right\rangle = \frac{1}{2\pi} \int_0^{2\pi} \left(\frac{\mathrm{d}\phi}{\mathrm{d}\theta} \right) \mathrm{d}\theta, \tag{5}$$

where, from Eq. (2), $\mathrm{d}\phi/\mathrm{d}\theta = (rB_\phi)/(R_0 B_\theta)$. The safety factor is proportional to the inverse of the rotational transform and measures the pitch of the field line. The dependence of the safety factor q_{eq} on the radius is dictated by the details of the equilibrium magnetic field, which in turn depends on the toroidal plasma current. The following expression describes in a satisfactory way typical nonmonotonic q-profiles of plasma discharges in tokamak experiments [Oda & Caldas, 1995]

$$q_{\mathrm{eq}}(r) = q_a \frac{r^2}{a^2} \left[1 - \left(1 + \beta' \frac{r^2}{a^2} \right) \times \left(1 - \frac{r^2}{a^2} \right)^{\mu+1} \Theta(a - r) \right]^{-1}, \tag{6}$$

where a is the plasma radius (slightly less then the tokamak minor radius b), q_a, β, and μ are parameters that can be chosen to fit experimentally observed plasma profiles ($\beta' = \beta(\mu+1)/(\beta+\mu+1)$), and Θ is the unit step function. We choose $q_a = 3.9$, $\beta = 2$ and $\mu = 1$, which results in a slightly nonmonotonic profile with a minimum near $y = 0.55$, as seen in Fig. 2. It is the presence of such a minimum that results in a violation of the condition $\partial r_{n+1}/\partial\theta_n \neq 0$, making $\mathbf{T}_e$ a nontwist map.

The ergodic limiter design we consider is a ring-shaped coil of width l, with m pairs of straight sections in the toroidal direction, with current I_l flowing in opposite senses for two adjacent segments (Fig. 1) [Martin & Taylor, 1984; McCool *et al.*, 1989; Caldas *et al.*, 1996; Portela *et al.*, 2003]. The effect of an ergodic limiter on an equilibrium configuration can be approximated by a sequence of delta function pulses at each piercing of a field line with the surface of section. Such a map has been described by Ullmann and Caldas [2000]:

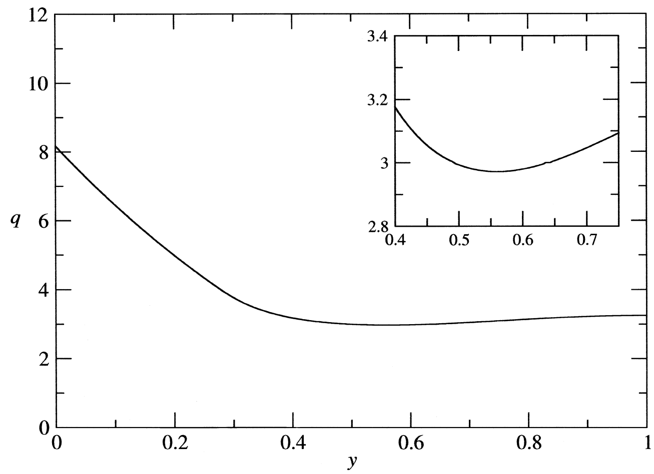

Fig. 2. Plot of the equilibrium safety factor profile with $q_a = 3.9$, $\beta = 2$ and $\mu = 1$. The inset emphasizes the minimum.

$$r_n = r_{n+1} + \frac{mCb}{m-1} \left(\frac{r_{n+1}}{b} \right)^{m-1} \sin(m\theta_n), \tag{7}$$

$$\theta_{n+1} = \theta_n - C \left(\frac{r_{n+1}}{b} \right)^{m-2} \cos(m\theta_n), \tag{8}$$

where $C = (2mla^2 I_l)/(R_0 q_a b^2 I_p)$ represents the perturbation strength due to the magnetic ergodic limiter. We denote this map by $(r_{n+1}, \theta_{n+1}) = \mathbf{T}_\ell(r_n, \theta_n)$, which can be derived from the mixed variable generating function

$$\mathcal{F}_\ell(r_{n+1}, \theta_n) = r_{n+1}\theta_n - \frac{Cb}{m-1} \left(\frac{r_{n+1}}{b} \right)^{m-1} \cos(m\theta_n), \tag{9}$$

with

$$\theta_{n+1} = \frac{\partial \mathcal{F}_\ell}{\partial r_{n+1}}, \quad r_n = \frac{\partial \mathcal{F}_\ell}{\partial \theta_n}, \tag{10}$$

where (r, θ), as previously stated, are related to (x, y).

Choosing $m = 3$, $l = 0.08\,\mathrm{m}$, and considering the TBR-1 parameters [Caldas *et al.*, 2002]: $a = 0.08\,\mathrm{m}$, $b = 0.11\,\mathrm{m}$, $R_0 = 0.3\,\mathrm{m}$, we have $C \approx 2.1 \cdot 10^{-1} I_l/I_p$. We note that the results we obtain are qualitatively similar for any tokamak because their equilibrium parameters satisfy the same scaling laws. In the following, we use the ratio between the limiter and plasma currents, $\epsilon = I_l/I_p$, to quantify the perturbation strength. This ratio varies from 0.1 to 0.3, assuring a small value for the perturbation strength.

The entire field line map is the composition of the two maps, $\mathbf{T} = \mathbf{T}_e \circ \mathbf{T}_\ell$, and because of the way the variable r_{n+1} appears in Eq. (7), we must solve for it at each iteration using a numerical scheme (Newton–Raphson method). Nevertheless, the map $\mathbf{T}$ is area-preserving and can describe field line behavior in tokamaks with ergodic limiters in a convenient and fast way, since we do not need to numerically integrate the field line equations over the whole toroidal revolution, in order to get the coordinates of a field line intersection with the Poincaré section [da Silva *et al.*, 2002].

Due to the toroidal correction in the equilibrium map $\mathbf{T}_e$, the flux surfaces do not coincide with nested cylinders (tori). This fact, along with the effect of the map $\mathbf{T}_\ell$, changes the $q(r)$-profile, so that it must be determined numerically. For the composed map $\mathbf{T}$, the $q(r)$-profile of an orbit (and of its flux surface) is given by

$$q^{-1} = \iota = \frac{1}{2\pi}\langle\theta_{n+1} - \theta_n\rangle = \lim_{n\to\infty}\frac{1}{2\pi}\frac{\theta_n}{n}, \qquad (11)$$

where θ_n is lifted (i.e. is not taken modulo 2π), q denotes the perturbed q, and ι is the rotational transform. For chaotic orbits this limit does not exist and q is not defined, which is responsible for the discontinuities in Fig. 7.

3. The Barrier

The phase portraits of Fig. 3 show a scenario of separatrix reconnection (e.g. [Howard & Hohs, 1984; del-Castillo-Negrete & Morrison, 1993; Petrisor,

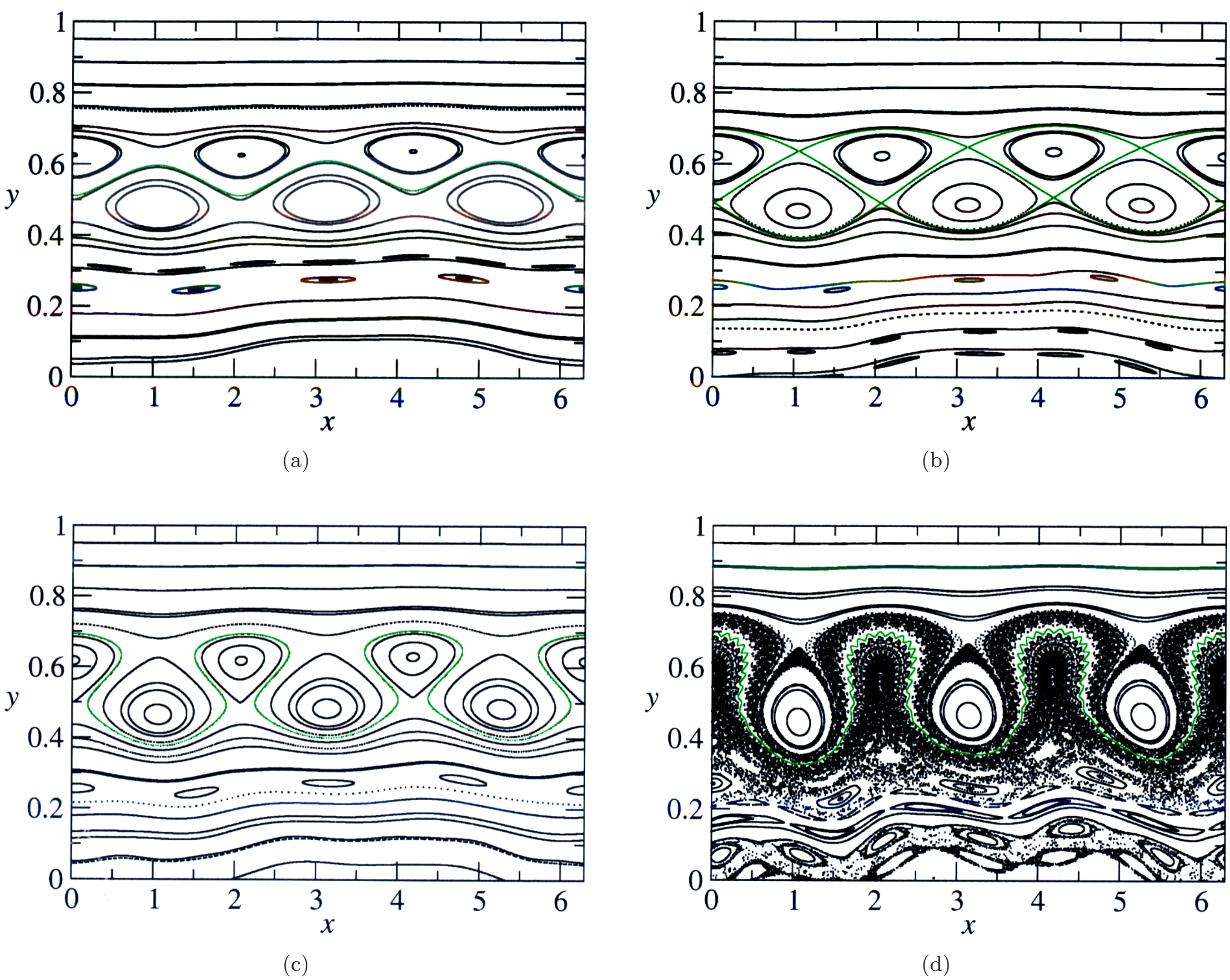

Fig. 3. Phase portraits exhibiting the reconnection scenario: depicted (a) for $\epsilon = 0.05$ are two island chains with invariant curves (green) between them; (b) for $\epsilon = 0.0635$ an heteroclinic connection (green); (c) for $\epsilon = 0.10$ the interchange of chain hyperbolic points (green); (d) for $\epsilon = 0.30$ the island chain disappearance in a bifurcation with a persistent barrier (green).

2002]), where the coordinates (x, y) [corresponding to (θ, r)] described in Sec. 2 are used. The nonmonotonicity of the q-profile with respect to y (radius) implies the existence of pairs of flux surfaces with the same q. Hence, a resonant perturbation gives rise to two island chains with the same period, separated by invariant curves (a); as the perturbation increases, the islands widen and the separatrices merge (b); then the chains interchange the separatrix trajectories that connect the hyperbolic points (c). Figure 3 also exhibits a bifurcation — the disappearance of an island chain due to the collision of its elliptic and hyperbolic points (d), as well as the rising and persistence of an invariant barrier separating the chaotic region in the phase space. This barrier is essentially formed by tori called *meanders*, which are not graphs over the x-axis. These meanders can only arise in nontwist maps [Wurm *et al.*, 2005]. Figure 3 shows there are invariant curves in the nonmonotonic region (see Fig. 6) and the chaos present is created in the monotonic region by the usual universal mechanism of torus destruction and island overlapping.

The barrier, observed in Fig. 3(d), turns out to be very robust; it is resistant to perturbations up to $\epsilon = 0.30$. We verify the barrier existence by finding an orbit that maps out an invariant curve. Using this procedure we increase the perturbation amplitude until no such orbits are found, and this establishes a lower bound on the critical perturbation, ϵ_c, necessary to destroy the barrier. We obtain $\epsilon_{\text{low}} = 0.30302$. An upper bound on the perturbation necessary for barrier destruction can be obtained by verifying whether or not a long trajectory (we use 10^{11} iterations for a chaotic orbit above the barrier region) passes through the barrier. Using

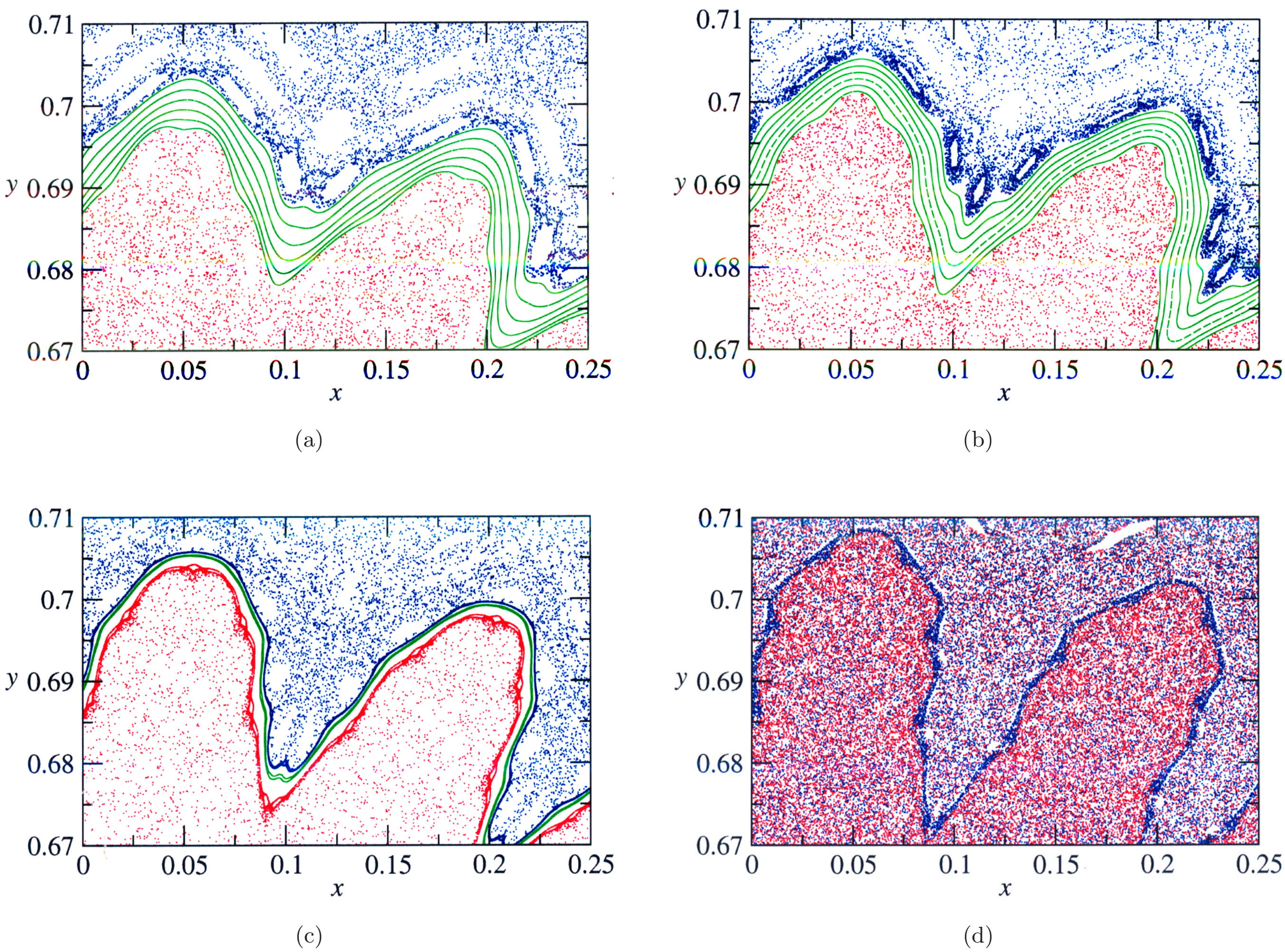

Fig. 4. Depiction of nonmonotonic barrier destruction. Phase portraits show one trajectory above (blue), one below (red) and some on (green) the barrier for the perturbation strengths (a) $\epsilon = 0.301$, (b) $\epsilon = 0.302$, (c) $\epsilon = 0.303$ and (d) $\epsilon = 0.304$, respectively. In case (d) the trajectories cross the barrier remnant.

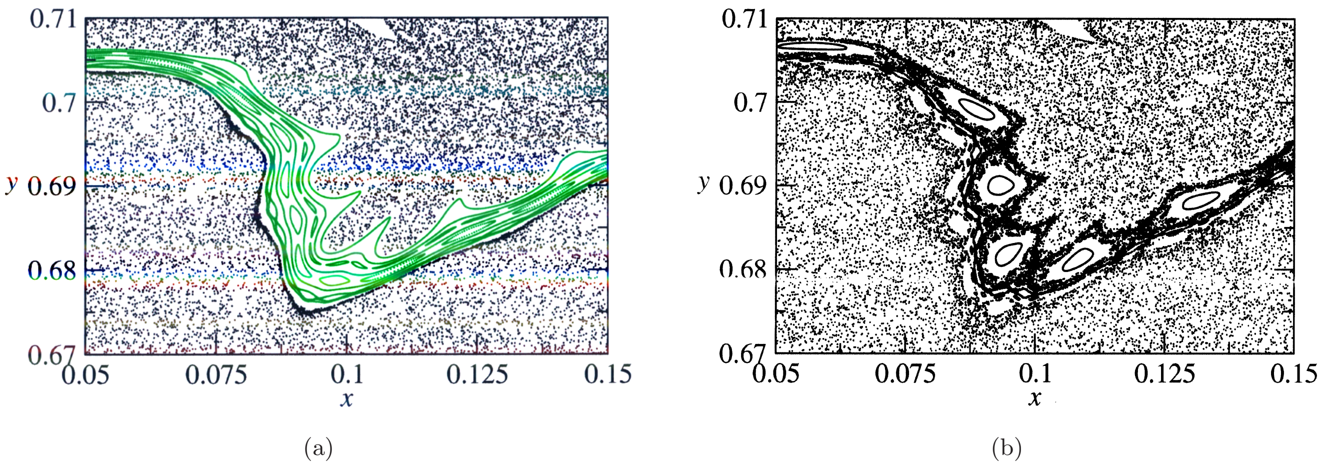

Fig. 5. Magnification of the barrier region showing (a) the islands inside the barrier (green) for $\epsilon = 0.3029$ and (b) for $\epsilon = 0.3031$ those that remain after its destruction.

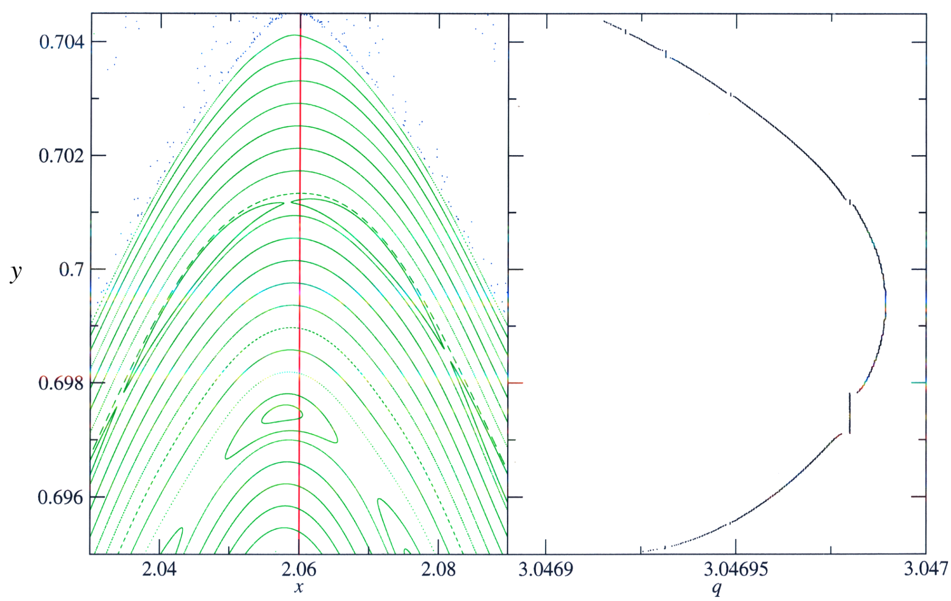

Fig. 6. Magnification of the barrier of Fig. 3(d) (left) and the corresponding safety factor profile $q(y)$, showing the maximum and plateaus of q.

this method we find $\epsilon_{\rm upp} = 0.30304$. Thus we can consider the critical perturbation to be the average of $\epsilon_{\rm low}$ and $\epsilon_{\rm upp}$, obtaining $\epsilon_{\rm c} = 0.30303$. Figures 4 and 5 show the barrier breaking.

An interesting feature of the profile $q(y)$ is the rising of a maximum with the perturbation ($\epsilon = 0.30$). This maximum is depicted in Fig. 6, along with the corresponding phase portrait that shows how it is related to the nonmonotonic invariant barrier [Wurm *et al.*, 2005]. Plateaus are also visible in the q-profile, particularly two of them related to the 454/149 island chains shown in the phase portrait. Figure 7(a) shows the global behavior of $q(y)$ in the presence of the perturbation. As is the case for monotonic systems [Ullmann & Caldas, 2000], plateaus and regions for which the limit of Eq. (11) is ill-defined are visible, the former corresponding to the resonances (islands) and the latter to chaotic regions for which the limit in Eq. (11) does not exist.

4. Transport

For perturbation strengths slightly above the critical value, orbits are not entirely free to wander over the whole chaotic sea. An effective remnant barrier still remains, with many orbits taking a very long time to pass through it.

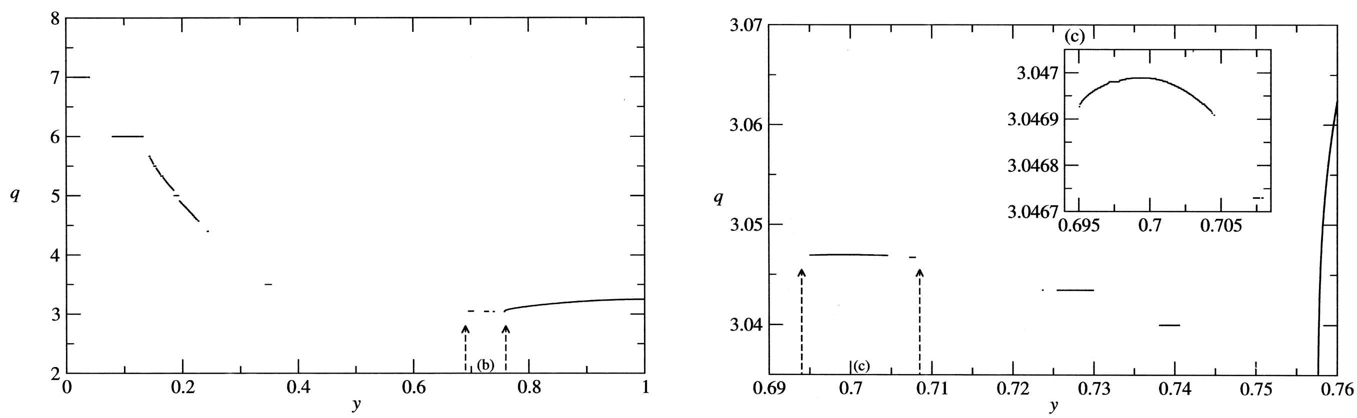

(a) (b)

Fig. 7. Plots of safety factor radial profiles at: (a) $x = 2.06$, (b) magnification of (a) at arrows, and (c) magnification of (b) at arrows. Plateaus correspond to islands resulting from the perturbation ($\epsilon = 0.30$), which also gives rise to chaotic regions where q is not defined. The zooming in (c) reveals that the apparent plateau in the barrier region has a local maximum (the other plateaus are really flat).

In order to quantify this effect, we consider orbits with initial conditions above the barrier and define F_n to be the fraction of the orbits remaining in this region after the nth iteration. Thus, since we compute the passage through the barrier using the radial coordinate, y, we call this *radial transport*.

Just above the critical parameter for barrier breaking, $\epsilon = 0.305$, we find (Fig. 8) for the first 2.5×10^5 iterations that the decay of the remaining fraction F_n is well described by $F_n = F_0 e^{-\beta n}$,

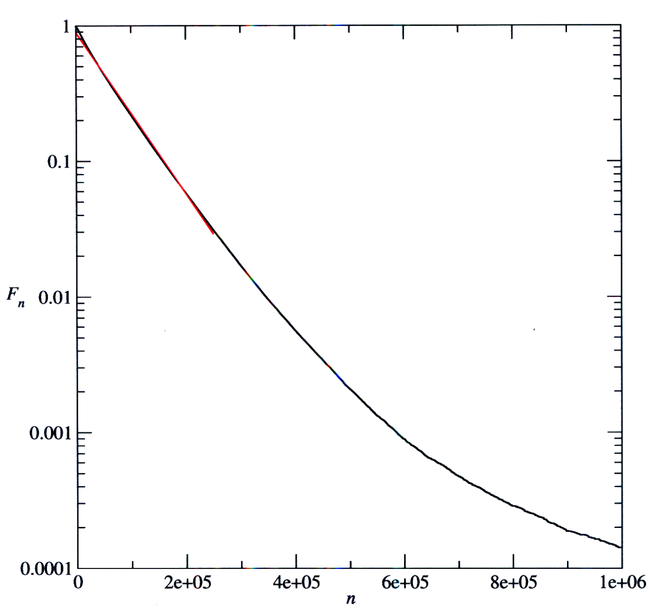

Fig. 8. Escape through the (effective) barrier for $\epsilon = 0.305$, using 10^6 initial conditions. For $F_n \gtrsim 0.05$, the remaining fraction decay is described by an exponential (red) with half-life of about $\sim 5 \cdot 10^4$ iterations. At late times a power law $\propto n^{-4}$ is a good approximation.

with $F_0 \approx 0.9$ and $\beta \approx -1.4 \times 10^{-5}$, and after that ($n > 2.5 \times 10^5$) it approximately follows a power law, $F_n \propto n^{-\gamma}$, where $\gamma \approx 4$. In the analysis of the F_n decay, we consider the time (number of iterations) for which the condition $F_n < 0.99$ is satisfied to be the beginning of the time series, because the amount of time orbits spend before starting to cross the barrier is more affected by the initial conditions than by the barrier itself.

We also calculate the average square radial displacement, σ_n^2, for an ensemble of N initial conditions at $y = y_0$,

$$\sigma_n^2 = \langle (y_i(n) - y_0)^2 \rangle = \frac{1}{N} \sum_{i=1}^{N} (y_i(n) - y_0)^2, \quad (12)$$

where $y_i(n)$ is the nth iteration of the ith initial condition and $\langle\ \rangle$ denotes the average over the ensemble.

For $\epsilon = 0.305$, Fig. 9 shows that σ_n^2 evolves linearly with time (the correlation coefficient between the data and a straight line is about 0.96) for the first 10^5 iterations characterizing a diffusive transport.

Since the orbits we take, i.e. ones with initial conditions placed far above the barrier, move gradually towards the barrier, which can be seen by taking phase space snapshots of the evolution, the linear behavior is not characteristic of the barrier alone. It is characteristic of the whole chaotic sea above it, where the field line shear is very low (see the small variation of q in Fig. 2). We attribute this unusual diffusive behavior to the stickiness around the many island chains present in the chaotic region.

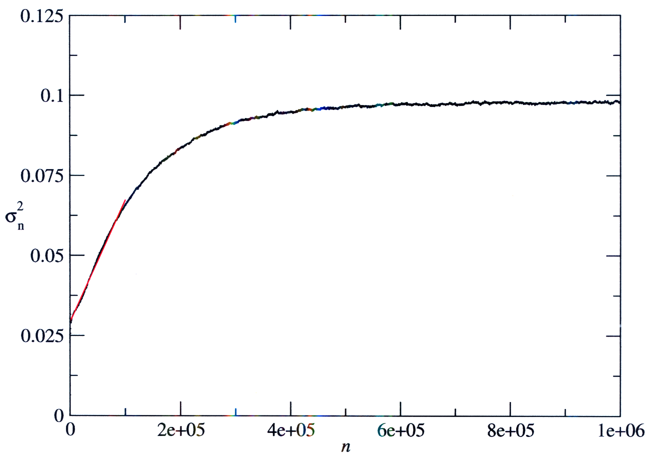

Fig. 9. Average square radial displacement time series as given by Eq. (12) for $\epsilon = 0.305$ (black) and 10^5 initial conditions located above (2, 0.75). For the first 10^5 iterations a straight line fit, $\langle (y_i(n) - y_0)^2 \rangle = 0.03 + 3.8 \cdot 10^{-8} n$ is shown (red) after the growth slows and reaches a plateau, corresponding to orbits filling the available phase space.

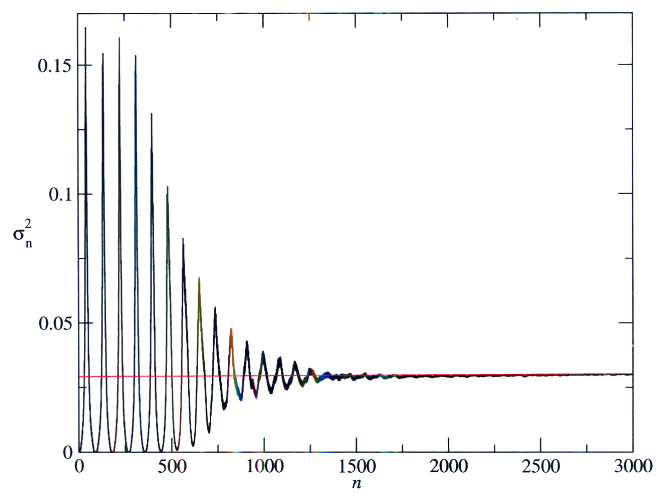

Fig. 10. Magnification of Fig. 9 showing the beginning of the average square displacement time series.

A similar diffusion has been observed after barrier breaking in the standard nontwist map [Corso & Lichtenberg, 1997]. After diffusing through the chaotic sea the orbits fill the available phase space, establishing a steady configuration with a constant average square displacement that corresponds to the plateau of Fig. 9.

Figure 9 gives information about radial diffusion: the diffusion through the barrier and the archipelago of many island chains. But, it turns out that this time series also yields information related to the transport *along* the barrier, the "poloidal transport." This information is contained in the "damped oscillations" present at the beginning of the average square displacement time series (Fig. 10).

Although chaos, loosely speaking, implies exponential divergence of nearby initial conditions, orbits initially very close remain nearby for some time, especially with the low divergence rate of the present system, which has a maximal Lyapunov exponent of about 10^{-2}. This happens for our point-concentrated initial conditions, which provides an explanation of the observed oscillations: because of stickiness, orbits tend to bypass the main island chain near them, as does the barrier itself, and the peaks of the oscillations correspond to the passage along the bottom of the islands [see Fig. 3(d)]. When the oscillations vanish, the average square displacement stabilizes in a plateau around 0.03, which corresponds to a state where points are distributed around the main island chain, i.e. the trajectories have scattered without penetrating the barrier.

Thus, the plateau indicates that orbits are distributed along the barrier and the large amplitude oscillations are related to nearby orbits. We interpret the decreasing amplitudes as the result of transport along the barrier. So, comparing the time scales for reaching the plateaus, about 0.03 and 0.1, we conclude that the diffusion along the barrier is about 200 times faster than through it.

5. Local Expansion for Low Limiter Current

In order to study more closely the role of the toroidal correction and the ergodic limiter perturbation, and to establish a comparison with the standard nontwist map [del-Castillo-Negrete & Morrison, 1993], we expand $\mathbf{T}$ around the location r^* of the equilibrium shearless curve. The standard nontwist map is a well-studied simple map that captures universal features of maps with a nonmonotonic q-profile. It is given by $x_{n+1} = x_n + c_1(1 - y_{n+1}^2)$ and $y_{n+1} = y_n - c_2 \sin(2\pi x_n)$, where c_1 is the profile parameter and c_2 measures the perturbation strength.

Because $2\pi/q(r) \gtrsim 1$ for $r < a$, to leading order, we can drop the a_1 term ($|a_1| \ll 1$) in Eq. (4), obtaining $\theta_{n+1} = \theta_n + 2\pi\alpha(r_{n+1})$, where $\alpha(r) := 1/q(r)$. Then, considering the shearless curve located at r^*, where $\mathrm{d}\alpha(r^*)/\mathrm{d}r = 0$, and defining

$$y' = r - r^* \ll r^*, \tag{13}$$

we can expand $\alpha(r_{n+1})$ in a Taylor series up to second order. This gives $\theta_{n+1} = \theta_n + 2\pi\alpha(r^*) + \pi\alpha''(r^*)y'^2_{n+1}$, with $\alpha'' := \mathrm{d}^2\alpha/\mathrm{d}r^2$, which can be rewritten as

$$\theta_{n+1} = \theta_n + c_1(1 - y^2_{n+1}), \tag{14}$$

where $c_1 := 2\pi\alpha(r^*)$ and

$$y' := \sqrt{\frac{-2\alpha(r^*)}{\alpha''(r^*)}}\, y =: b'y. \tag{15}$$

Using $|a_1| \ll 1$ in Eq. (3) gives $r_{n+1} = r_n(1 + a_1 \sin\theta_n)$, and considering Eqs. (13) and (15) and neglecting second order terms, results in

$$y_{n+1} = y_n - c_2 \sin(\theta_n), \tag{16}$$

with $c_2 \equiv -a_1 r^*/b'$. Equations (14) and (16) are the standard nontwist map.

Similarly, we expand the limiter map $\mathbf{T}_\ell$ of Eqs. (7) and (8). We do this by inserting $r = r^* + y$ into the generating function expressions of Eq. (10) and expanding up to second order, obtaining the approximate generating function

$$\tilde{\mathcal{F}}_\ell(y_{n+1}, \theta_n) = y_{n+1}\theta_n - \frac{Cb}{m-1}\left(\frac{r^*}{b}\right)^{m-1} \times \left[1 + \frac{m-1}{r^*}y_{n+1}\right]\cos(m\theta_n). \tag{17}$$

If we further drop the term $y_{n+1}(m-1)/r^*$, we obtain

$$y_{n+1} = y_n - F(r^*)\sin(m\theta_n), \tag{18}$$

$$\theta_{n+1} = \theta_n, \tag{19}$$

with

$$F(r) = \frac{mCb}{b'(m-1)}\left(\frac{r}{b}\right)^{m-1}. \tag{20}$$

So, the approximate composed map is

$$y_{n+1} = y_n - c_2\sin(\theta_n) - c_3\sin(m\theta_n), \tag{21}$$

$$\theta_{n+1} = \theta_n + c_1(1 - y^2_{n+1}), \tag{22}$$

where $c_3 = F(r^*)$.

Therefore, the local version of the nontwist model used in this work consists of the standard nontwist map of Eqs. (14) and (16), where the perturbative term $c_2\sin(\theta)$ comes from the toroidal effects, plus an additional perturbation, $c_3\sin(m\theta_n)$, due to the ergodic limiter. The twist version of this map (the standard map with the same c_3 term) was considered by Greene and Mao [1990] to study the torus break-up in a co-dimension two system. They observed torus breakup different from that of the standard map, and it is expected for $m \neq 1$ that there will be a new universality class for torus break-up, one different from that of the standard nontwist map [del-Castillo-Negrete *et al.*, 1997].

For the parameter values used in this work we have: $c_2 \approx 2 \times 10^{-3}$, $c_1 \approx 2.1$, and $c_3 \sim \epsilon/100$. So, the ϵ range mostly used in this work is $0.1 < \epsilon < 0.3$, and c_2 and c_3 are of the same order of magnitude, which means that even locally neither the effect of the geometry nor the limiter action can be neglected. Moreover, it should be the coupling of these two effects that allows small amplitude perturbations ($\sim 10^{-3}$) to create the configuration of Fig. 3(d). This configuration is similar to the one obtained in [Wurm *et al.*, 2004] for the standard nontwist map ($c_3 = 0$ in Eq. (21)) for $c_2 = 0.5$ and a similar c_1. In our model this corresponds to a high toroidal correction without the limiter perturbation. Thus, in the considered approximation, our map describes the interaction between two resonances with $m = 1$ (due to the toroidal geometry) and $m = 3$ (induced by the ergodic limiter). In this work we focused on this $m = 3$ perturbation, which is resonant in the shearless region. Nevertheless the $m = 1$ mode still affects the transport barrier structure.

6. Conclusions

In this paper we have presented a nontwist map model for the magnetic field line dynamics, a model that exhibits experimentally observed transport barriers. Such transport barriers are desirable because they impede particle loss and improve confinement. The barriers of our map model were found to be very robust, demanding strong perturbation to be destroyed, and even after their break-up the transport turned out to be diffusive. This diffusive transport occurs not only through the remnant barrier that remains but throughout the whole chaotic sea. We attribute this behavior to the archipelago of higher order island chains present in the chaotic region, which are due to the nonmonoticity of the safety factor profile $q(y)$

We also showed that, although the equilibrium q-profile has a minimum, the barrier that arises in the nonmonotonic region, due to the perturbation, corresponds to a local maximum. It was found that for a perturbation strength slightly above the critical value, a population of initial conditions located on one side of the effective barrier passes through it diffusively at an exponential rate with half-life of about 5×10^4 iterations. The "poloidal" transport, i.e. the transport along the barrier, was found to be 200 times faster than through it. Finally, we verified that the map used in this work is locally equivalent to the standard nontwist map (near the shearless curve) with an additional perturbation due to the ergodic limiter. And, even when two resonances are present, the map has behavior akin to that of the standard nontwist map.

Acknowledgments

This work was made possible through partial financial support from the following Brazilian research agencies: FAPESP and CNPq. The authors would like to acknowledge Elton C. da Silva for valuable discussions. One of the author P. J. Morrison, was supported by the US DOE Grant DE–FG03–96ER–54346.

References

Caldas, I. L., Pereira, J. M., Ullmann, K. & Viana, R. L. [1996] "Magnetic field line mappings for a tokamak with ergodic limiters," *Chaos Solit. Fract.* **7**, 991–1010.

Caldas, I. L., Viana, R. L., Araujo, M. S. T., Vannucci, A., da Silva, E. C., Ullmann, K. & Heller, M. V. A. P. [2002] "Control of chaotic magnetic fields in tokamaks," *Braz. J. Phys.* **32**, 980–1004.

Corso, G., Oda, G. & Caldas, I. L. [1997] "Minimizing chaos during the reconnection process," *Chaos Solit. Fract.* **8**, 1891–1900.

Corso, G. & Lichtenberg, A. J. [1999] "Threshold to global diffusion in a nonmonotonic map with quadratic nonlinearity," *Physica D* **131**, 1–16.

Davidson, M. G., Dewar, R. L., Gardner, H. J. & Howard, J. [1995] "Hamiltonian maps for heliac magnetic islands," *Aust. J. Phys.* **48**, 871–886.

da Silva, E. C., Caldas, I. L. & Viana, R. L. [2002] "Bifurcations and onset of chaos on the ergodic magnetic limiter mapping," *Chaos Solit. Fract.* **14**, 403–423.

del-Castillo-Negrete, D. & Morrison, P. J. [1993] "Chaotic transport by Rossby waves in shear flow," *Phys. Fluids A* **5**, 948–965.

del-Castillo-Negrete, D., Greene, J. & Morrison, P. J. [1997] "Renormalization and transition to chaos in area preserving nontwist maps," *Physica D* **100**, 311–329.

Egydio de Carvalho, R. & Ozório de Almeida, A. M. [1992] "Integrable approximation to the overlap of resonances," *Phys. Lett. A* **162**, 457–463.

Greene, J. M. & Mao, J. [1990] "Higher-order fixed points of the renormalisation operator for invariant circles," *Nonlinearity* **3**, 69–78.

Howard, J. E. & Hohs, S. M. [1984] "Stochasticity and reconnection in Hamiltonian systems," *Phys. Rev. A* **29**, 418–421.

Karger, F. & Lackner, K. [1977] "Resonant helical divertor," *Phys. Lett. A* **61**, 385–387.

Levinton, F. M. *et al.* [1995] "Improved confinement with reversed magnetic shear in TFTR," *Phys. Rev. Lett.* **75**, 4417–4420.

Lichtenberg, A. J. & Lieberman, M. A. [1992] *Regular and Chaotic Dynamics* (Springer, NY).

Martin, T. J. & Taylor, J. B. [1984] "Ergodic behavior in a magnetic limiter," *Plasma Phys. Contr. Fusion* **26**, 321–340.

Mazzucato, E. *et al.* [1996] "Turbulent fluctuations in TFTR configurations with reversed magnetic shear," *Phys. Rev. Lett.* **77**, 3145–3148.

McCool, S. C., Wootton, A. J., Aydemir, A. Y. *et al.* [1989] "Electron thermal confinement studies with applied resonant fields on TEXT," *Nucl. Fus.* **29**, 547–562.

Morrison, P. J. [2000] "Magnetic field lines, Hamiltonian dynamics, and nontwist systems," *Phys. Plasmas* **7**, 2279–2289.

Oda, G. A. & Caldas, I. L., [1995] "Dimerized island chains in tokamaks," *Chaos Solit Fract.* **5**, 15–23.

Petrisor, E. [2002] "Reconnection scenarios and the threshold of reconnection in the dynamics of non-twist maps," *Chaos Solit. Fract.* **14**, 117–127.

Portela, J. S. E., Viana, R. L. & Caldas, I. L. [2003] "Chaotic magnetic field lines in tokamaks with ergodic limiters," *Physica A* **317**, 411–431.

Portela, J. S. E., Caldas, I. L., Viana, R. L. [2007], "Exit basins in tokamaks with the Wada property," *Int. J. Bifurcation and Chaos* **17**(11).

Strait, E. J. *et al.* [1995] "Enhanced confinement and stability in DIII-D discharges with reversed magnetic shear," *Phys. Rev. Lett.* **75**, 4421–4424.

Ullmann, K. & Caldas, I. L. [2000] "A sympletic mapping for the ergodic magnetic limiter an its dynamical analysis," *Chaos Solit. Fract.* **11**, 2129–2140.

Viana, R. L. & Caldas, I. L. [1992] "Peripheral stochasticity in tokamak with an ergodic magnetic limiter," *Z Naturforsch* **47**, 941.

Wesson, J. [1987] *Tokamaks* (Oxford University Press, Oxford).

Wurm, A., Apte, K. & Morrison, P. J. [2004] "On reconnection phenomena in the standard nontwist map," *Braz. J. Phys.* **34**, 1700–1706.

Wurm, A., Apte, A., Fuchss, K. & Morrison, P. J. [2005] "Meanders and reconnection collision sequences in the standard nontwist map," *Chaos* **15**, 023108.